Structure *14*, 75–86, January 2006 ©2006 Elsevier Ltd All rights reserved DOI 10.1016/j.str.2005.09.014

Structure and Interactions at the Viral Surface of the Envelope Protein E1 of Semliki Forest Virus

Alain Roussel,[1,3,4] Julien Lescar,[1,3,5] Marie-Christine Vaney,[1] Gisela Wengler,[2] Gerd Wengler,[2] and Félix A. Rey[1,6,*]
[1] Laboratoire de Virologie Moléculaire and Structurale
UMR 2472/1157 CNRS-INRA and IFR 115
Avenue de la Terrasse
91198 Gif-sur-Yvette Cedex
France
[2] Institut of Virology
University of Giessen
35390 Giessen
Germany

Summary

Semliki Forest virus (SFV) is enveloped by a lipid bilayer enclosed within a glycoprotein cage made by glycoproteins E1 and E2. E1 is responsible for inducing membrane fusion, triggered by exposure to the acidic environment of the endosomes. Acidic pH induces E1/E2 dissociation, allowing E1 to interact with the target membrane, and, at the same time, to rearrange into E1 homotrimers that drive the membrane fusion reaction. We previously reported a preliminary Cα trace of the monomeric E1 glycoprotein ectodomain and its organization on the virus particle. We also reported the 3.3 Å structure of the trimeric, fusogenic conformation of E1. Here, we report the crystal structure of monomeric E1 refined to 3 Å resolution and describe the amino acids involved in contacts in the virion. These results identify the major determinants for the E1/E2 icosahedral shell formation and open the way to rational mutagenesis approaches to shed light on SFV assembly.

Introduction

Semliki Forest virus (SFV) belongs to the alphavirus genus in the *Togaviridae* family of small, enveloped, messenger-sense single-stranded RNA viruses (Weaver et al., 2000). It has been used as a model to unveil the endocytotic entry route used by many pathogenic microorganisms (Helenius et al., 1980). The alphavirus morphology has been studied extensively by using biochemical, genetic, and structural approaches. The virions are icosahedrally symmetric particles with a glycoprotein cage enclosing a roughly spherical viral membrane (Mancini et al., 2000; Paredes et al., 2001; Zhang et al., 2002). Inside the membrane, the nucleocapsid (NC), a second icosahedrally ordered structure matching the symmetry of the outer cage, packs the roughly 12 kb long genomic RNA. The protein components of the virion display specific interactions to ensure proper particle assembly, budding, and maturation during exit from the infected cell, as well as receptor binding, endosomal uptake, and triggering of membrane fusion during the invasion of a new cell (see Schlesinger and Schlesinger, 2001 and references therein for a comprehensive review on alphavirus biology).

The alphavirus structural proteins are translated from a subgenomic messenger RNA with a single open reading frame coding for the polyprotein precursor C-p62-6K-E1, which undergoes cotranslational cleavage to release its four constituent polypeptides. C forms the icosahedral NC core structure underneath the viral membrane, encasing the viral genome; p62 is a precursor of the mature E2 protein, which is responsible for receptor recognition when infecting a new cell; E1 is responsible for triggering fusion of the viral and target cell membranes during entry; and, finally, the small intervening 6K protein is necessary for efficient particle budding (Liljestrom et al., 1991) and is present at low levels in virions (Gaedigk-Nitschko and Schlesinger, 1990; Lusa et al., 1991).

Both p62 and E1 are type I proteins containing a single transmembrane (TM) segment, which, in the case of p62, is followed by a small, cytosolic C-terminal tail. Protein p62 binds to E1—most likely cotranslationally—in the ER and acts as a chaperone for folding E1 in a membrane fusion-competent conformation (Andersson et al., 1997; Garoff et al., 1994). The p62/E1 heterodimer is then transported to the plasma membrane, and, during this process, p62 is cleaved by furin (Zhang et al., 2003), a TGN resident protease, to yield mature E2 and E3 glycoproteins (de Curtis and Simons, 1988; Watson et al., 1991). E3 is derived from the N-terminal end of p62 and remains bound to E2 in virions only for some strains of SFV. Mature E1/E2 heterodimers accumulate at the plasma membrane (Salminen et al., 1992) and interact with the NC cores present in the cytoplasm via the cytosolic tail of E2. This interaction leads to morphogenesis and budding of infectious virions (Skoging et al., 1996).

Cleavage of p62 activates the alphavirus fusogenic potential, yielding a metastable E1/E2 heterodimer that dissociates upon exposure to mildly acidic pH, allowing E1 to bind to the target membrane via its fusion peptide (reviewed by Bron et al., 1993; Kielian et al., 2000). Heterodimer dissociation is followed by a fusogenic conformational change of E1 to form a homotrimer in which the E1 subunits adopt a hairpin conformation, bringing together the fusion peptide and the TM segment at one end of the molecule (Gibbons et al., 2004). The membrane fusion reaction occurs as a cooperative process involving lateral interactions between E1 homotrimers that distort target and viral membranes in such a way that lipid merging is induced (Gibbons et al., 2003, 2004).

E1/E2 heterodimers form trimers that are the building blocks of the glycoprotein cage of the virion (von Bonsdorf and Harrison, 1975, 1978) (also, see the review by Garoff et al., 1994). These $(E1/E2)_3$ complexes make 80

*Correspondence: rey@vms.cnrs-gif.fr
[3] These authors contributed equally to this work.
[4] Present address: Centre de Biophysique Moléculaire, F45071 Orléans Cedex 2, France.
[5] Present address: School of Biological Sciences, Nanyang Technological University, 60 Nanyang Drive, Singapore 637551, Singapore.
[6] Present address: Virology Department, Institut Pasteur, 25 rue du Dr. Roux, 75015 Paris, France.

trimeric spikes at the virus surface that project from a protein scaffold of icosahedral architecture with triangulation T = 4 (Caspar and Klug, 1962). The TM segments of E1 and E2 cross the membrane together, roughly at the vertices of the triangular base of the spikes. The cytoplasmic tail of E2 makes one-to-one interactions with the NC, which also exhibits a T = 4 icosahedral organization, resulting in a total of 240 identical C/E2 contact sites (Zhang et al., 2002, Lee et al., 1996).

We previously reported the Cα trace of the E1 polypeptide built from a 3.5 Å resolution electron density map calculated from X-ray diffraction data (Lescar et al., 2001). The crystals were anisotropic, and the diffraction was of poor quality and did not allow further refinement of the polypeptide trace at the time. This preliminary model was fitted into a 3D reconstruction at 9 Å resolution of the SFV particle calculated by cryo-EM and image processing (Mancini et al., 2000). The overall arrangement of the E1 molecules in the virus particle was interpreted with the help of this model, and the remainder of the density was attributed to E2 (Lescar et al., 2001). The resulting assignment was independently confirmed by 3D reconstructions of glycosylation-deletion mutants of a related alphavirus, Sindbis virus (Pletnev et al., 2001; Zhang et al., 2002). However, the identity of the amino acid side chains involved in the contacts was not provided because the model was only preliminary. Here, we present the results of the crystallographic refinement of the E1 structure, by using diffraction data partially extending to 3 Å resolution. This model contains all of the atoms of the 384 N-terminal amino acids of the E1 ectodomain (out of 413 residues upstream of the TM segment—i.e., lacking most of the "stem" region of the ectodomain, residues 382–413). Placement of the refined model into the cryo-EM reconstruction now allows for visualization of the E1 residues involved in lateral E1/E1 and E1/E2 contacts that form the external glycoprotein cage of the particle. This model was also used to interpret the higher-resolution 3D reconstruction of Sindbis virus described in the accompanying manuscript (Mukhopadhyay et al., 2006). These results provide a rational basis for site-directed mutagenesis experiments to validate the importance of the interactions described for assembly and particle formation.

Results and Discussion

Structure Determination

The monomeric, soluble ectodomain of E1 (termed "E1-ΔS," containing amino acids 1–390 out of 438 in the intact protein) was obtained by controlled subtilisin treatment of the SFV glycoproteins detergent solubilized from purified virus preparations; it crystallizes in the hexagonal space group $P6_422$ (Wengler et al., 1999). The diffraction pattern is very anisotropic, with some crystals diffracting to about 2.4 Å resolution along the direction of the 6_4 hexagonal axis, but only to 3.7 Å in perpendicular directions. The crystals contain a single E1-ΔS monomer in the asymmetric unit and are generally nonisomorphous to each other. The crystal structure was determined by MIR and MAD methods, followed by multicrystal averaging, as described in Lescar et al. (2001), by using diffraction data from several nonisomorphous crystals with cell parameters differing by 2%–3%. For the crystallographic refinement reported here (Table 1), we chose one crystal in which the anisotropy was less marked, diffracting to 3 Å in the good direction and to about 3.3–3.5 Å in the perpendicular plane. The anisotropy is reflected in the drop in completeness of the diffraction data represented in Table 2. Several controls to independently identify the disulfide bonds of the molecule and the side chains containing a carboxylate group (aspartate and glutamate residues) were carried out (see Figures S1–S3 in the Supplemental Data available with this article online). Finally, the trace was further confirmed by the independently determined 3.3 Å resolution

Table 1. Crystallographic and Refinement Statistics

Data Collection Statistics	
Space group	$P6_422$
Cell parameters (Å, °)	a = 79.38, b = 79.38, c = 335.91, γ = 120
Resolution (Å)	39.0–3.0 (3.21–3.00)[a]
Measured reflections	82,854
Unique reflections	10,666
Redundancy	7.8 (5.5)[a]
Completeness (%)	87.6 (76.1)[a]
I/σ(I)	8.0 (5.4)[a]
R_{merge} (%)	7.5 (12.4)[a]
Refinement Statistics	
R factor (%)	26.6 (38.0)[a]
R_{free} (%)	31.8 (53.7)[a]
Number of amino acid residues	384
Number of water molecules	88
Number of protein non-hydrogen atoms	3023
Rms deviations from ideal value	
Bond lengths (Å)	0.006
Bond angles (°)	1.028
Chirality	0.061
Ramachandran statistics	
Most favored region (%)	78.6
Additional allowed region (%)	20.5
Generously allowed region (%)	0.6
Disallowed region (%)	0.3
$<B\ average>_{all\ atoms}$	
All domains	63.7
DI + DII	54.7
DIII	101.6

R factor = $\Sigma|F_o - F_c|/\Sigma|F_o|$. $R_{free} = \Sigma|F_o - F_c|/\Sigma|F_o|$, calculated using 10% of the data selected randomly from the observed reflections. F_o and F_c are, respectively, the observed and calculated structure factor amplitudes.
[a] Values in parentheses refer to the highest-resolution shell.

Table 2. Statistics per Resolution Shell

Resolution Range (Å)[a]	Completeness (%)	R_{free} Factor (%)
12.90	91.85	0.30
7.66	100.00	0.28
5.97	99.91	0.31
5.06	100.00	0.23
4.47	99.04	0.31
4.05	92.89	0.29
3.72	83.60	0.34
3.47	79.54	0.39
3.24	76.46	0.38
3.07	76.78	0.49

[a] Completeness at the highest-resolution shell reflects the anisotropy of the crystals. The overall resolution range is 39–3 Å, and it was divided in ten resolution shells spanning 1/39 to 1/3 $Å^{-1}$. The value quoted is $1/d_i$, where d_i is the center of the i^{th} resolution shell.

structure of the detergent-solubilized E1 ectodomain in its acidic pH homotrimeric (HT) conformation (this form of the protein was called E1*HT) (Gibbons et al., 2004). The experimental 3.3 Å MIR/SIR electron density map of E1*HT was of very good quality thanks to the very high anomalous phasing power of four holmium atoms tightly bound per trimer. In addition, the crystals of the trimer contained one E1*HT in the unit cell, allowing 3-fold noncrystallographic averaging. The electron density of E1*HT confirmed the amino acid assignment of each of the three domains of E1, which retain the same fold observed in the monomer, but change the relative orientation and positioning with respect to each other. All of the domain III (DIII) region, and the DIII proximal region of DI, display very high-temperature factors in the E1-ΔS monomer crystals (see Table 1 and Figures S3 and S4), and the model could only be refined by making extensive use of the TLS algorithm implemented in the REFMAC program (Winn et al., 2003). A superposition of the backbone of the old and the new traces is provided in Figure S3, highlighting the regions where the biggest differences were found. Figure S4 provides a plot of the individual B factors and the atomic displacement parameters, showing a sharp increase of the latter for the 100 C-terminal residues (which make up domain III). Not surprisingly, this was the region of highest uncertainty in the previously published initial trace of the molecule. Fortunately, this region turned out to be the best-ordered segment in the crystals of E1*HT.

The limited resolution and the anisotropy of the diffraction data (Table 2), which reflects an inherent flexibility of the molecule, combined with the absence of noncrystallographic symmetry, limit the refinement of the E1-ΔS monomer to an R_{free} of 31%–32% (Table 1). Nonetheless, the independent tests described above make us confident that we have correctly interpreted the experimental electron density to produce the current atomic model and, by extension, the pseudo atomic model of the E1 layer of the virus particle presented in this manuscript.

Description of the Molecule

Figure 1 displays the secondary structure of E1, color-coded according to domains (DI–DIII) as introduced initially for the flavivirus E protein. The connectivity is more easily followed by using the simplified topology diagram of Figure 1B. The model contains 384 residues (out of the 390 present in the crystallized E1 proteolytic fragment) (Wengler et al., 1999). There are a total of 29 β strands, a short α helix, and three one-turn 3/10 helices (labeled η1–3). For the β strands, we adopted the nomenclature introduced to describe the structure of the tick-borne encephalitis (TBE) virus E glycoprotein (Rey et al., 1995), with uppercase letters with a "0" subindex to indicate strands from DI, and lower and uppercase letters to denote strands from DII and DIII, respectively. The short α helix present in E1 is homologous to the second short α helix of the TBE E protein and was labeled identically (αB) to keep the same nomenclature. Figure 1C shows a sequence alignment of E1 from seven representative alphaviruses, including one representative of the more distant fish alphaviruses (SDV, last sequence) that are apparently not vector-borne (all the others being insect-borne). Interestingly, fish alphaviruses have three insertions along the primary sequence, numbered in gray below the alignment, which appear to make a more bulky region of the protein at the sites indicated by gray arrows in Figure 1A. These insertions apparently contact each other on one side of the protein, in the area described below as part of the contact with E2 in the virus particle. It is possible that there are matching insertions/deletions in E2 to compensate for these insertions, but a crystal structure of E2 is needed for further analysis.

Individual Domains

Domain I

DI is an eight-stranded β sandwich with simple up-and-down topology. Compared to the flavivirus E protein, DI lacks the N-terminal strand A_0, which runs parallel to strand C_0 at a side of the antiparallel DI β sandwich. In E1, the C_0D_0 hairpin projects out of the β sandwich to interact with the DI/DIII linker (see below). DI contains the only N-linked carbohydrate of the glycoprotein, the density of which is apparent in the electron density maps. The first glycosamino-glycan residue was modeled, but the atoms refined to very high B factors and resulted in an increase of the R_{free}; thus, the sugar was removed from the final model. The glycosylation site is indicated by a yellow fan in the E_0F_0 loop in Figures 1A and 1C. Most alphavirus have a glycosylation site in this loop, except for the fish alphaviruses, in which the glycan is on strand D_0, on the same face of the DI β sandwich. Interestingly, the E_0F_0 loop also carries a glycosylation site in protein E from most flaviviruses. Some alphaviruses, like Sindbis virus, carry a second glycan, located between helices αB and η2 (see Figure 1C).

Domain II

DII is formed by two long excursions of the polypeptide chain that appear as insertions in the D_0E_0 and H_0I_0 loops of DI. These two elements are drawn in orange and yellow in Figure 1A. Both segments are stabilized by disulfide (SS) bonds. SS bonds 1–4 (labeled in Figures 1A and 1C) are internal to the orange segment, and SS bond 5 lies within the yellow segment, stabilizing the kl β hairpin at the base. A central feature of DII is a short six-stranded antiparallel β sheet, gfeahh′, (labeled as "central β sheet" in Figure 1B) extending roughly parallel to the long axis of the domain. This structure bridges DI with the elongated fusion loop-bearing β sandwich (FLBS, labeled in Figure 1B), formed by the apposed bdc β sheet and the ij β hairpin at one end of the molecule. The ij loop is longer than in flavivirus E, and it interacts with the cd loop (i.e., the fusion peptide loop). The central DII β sheet packs, on one side, against the long gh loop (running below in the orientation of Figure 1A) and against the kl β hairpin on the other. The gh loop contains one of the most conserved sequence elements of the polypeptide chain, comparable to that of the fusion cd loop, as can be seen in the alignment of Figure 1C.

Domain III

This domain is a member of the immunoglobulin (Ig) superfamily and is most similar to the tandemly repeated Ig-like domains of bacterial proteins that mediate adhesion between mammalian cells and pathogenic bacteria, like intimin from *E. coli* enteropathogenic strains (Luo et al., 2000) or invasin from *Yersinia pseudotuberculosis* and *Y. enterocolitica* (Hamburger et al., 1999).

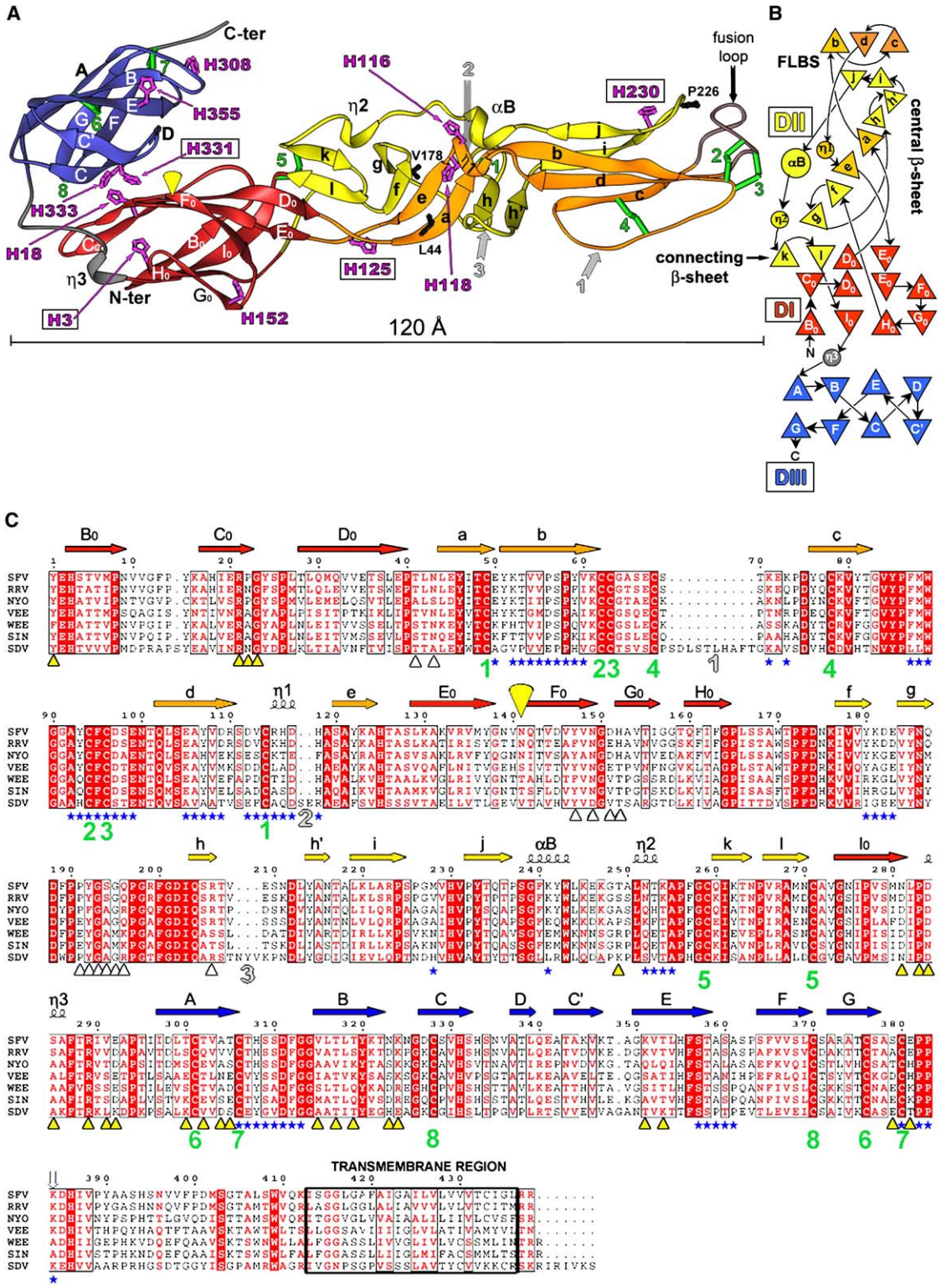

Figure 1. Structure of SFV E1

(A) Ribbon diagram colored according to domains, by using the standard class II color coding (red, yellow, and blue for DI, DII, and DIII, respectively), except that DII is colored yellow and orange to distinguish the two insertions into DI loops (at D_0E_0 and H_0I_0) that make up this domain, and the fusion peptide is brown. The SS bonds are drawn as green cylinders and are labeled from 1 to 8. A yellow fan denotes the single glycosylation site at position 141. All of the histidine side chains present in the structure are drawn in magenta and labeled; conserved ones are framed (note the cluster of three histidines at the DI/DIII interface, around His331). The side chains of mutants that affect the lipid dependence of the fusion activity of E1 are drawn and labeled in black. Numbered gray arrows point to the location of E1 insertions in the more distant fish alphaviruses (see [C]). (B) Topological diagram of E1, drawn with TOPS (Flores et al., 1994) and colored according to domains. The domains are labeled in colored font (matching the class II scheme). In DII, the central and connecting β sheets and the fusion loop-bearing β sandwich (FLBS) are labeled in black.

The latter mediates bacterial entry into eukaryotic cells by binding to integrins at the target cell surface. The DALI score (Holm and Sander, 1996) of the structural alignment between DIII and intimin domain 1 is 7.7, and 82 (out of the 88) Cα atoms of DIII superpose with 2.7 Å rms. In such alignment, the homologous flavivirus protein E DIII scores in the 12th position, with a DALI score of 6.0 and with 69 residues superposing with 2.4 Å rms.

A distinguishing feature of E1/DIII is that, unlike its most similar relatives present in cell adhesion molecules, which have been classified as belonging to the "I set" of the Ig superfamily constant-like domains (Harpaz and Chothia, 1994), it is stabilized by three conserved SS bonds. In addition, the polypeptide chain after strand C first makes a short D strand, hydrogen bonded antiparallel to strand E—as in a standard constant Ig domain, and then switches to the opposite sheet to run antiparallel to strand C, like a C′ strand in a variable Ig domain. The strands were therefore labeled accordingly, even if strand C′ comes after D in the sequence (Figure 1C). An additional feature is that there is no A′ strand like in the other I set members, but the end of strand G instead switches from the CFG sheet to run parallel to strand A in the opposite ABED sheet for a short run (two hydrogen bonds). Strand G is further tied to strand A by two of the three SS bonds present in DIII (SS 6 and 7 in Figure 1).

Interdomain Contacts

The Hinge Region

DI and DII do not display a sharp boundary. The connection between them is made by the intervening kID_0E_0 sheet (labeled "connecting sheet" in Figure 1B), in which we have arbitrarily assigned one half—the kl hairpin—to DII and the other half to DI, since these strands are a continuation of D_0 and E_0 of DI. This flexible region, in which the kl β hairpin packs against the η2 helix and the fg β hairpin of the central β sheet, has been called "the hinge" (Rey et al., 1995; Lescar et al., 2001). Flexibility of the molecule about this area was evident during the fit of the model into the cryo-EM reconstruction, where a 10° rotation had to be applied between DI and DII about an axis passing in between the connecting and central β sheets (Lescar et al., 2001) to fit the cryo-EM density. Furthermore, the different nonisomorphous crystals of E1 used to solve the structure displayed different angles between DI and DII. Finally, a rotation of DII about the same axis was also observed in the structure of the low-pH homotrimer of E1 (Gibbons et al., 2004). Indeed, the structure of E1*HT shows a slightly different packing of the central β sheet against both the kl hairpin and the conserved gh loop underneath, suggesting that the central sheet is flexible enough to accommodate different angles between the FLBS and DI. In the case of the homologous E protein from dengue virus (DV), a bound detergent molecule was observed in precisely this region (Modis et al., 2003), altering the local conformation of the molecule. In the presence of detergent, the kl hairpin of DV E switches to the central sheet, extending it by two more strands. The hinge region of DV E has also been observed in several conformations, depending on the crystal packing (Modis et al., 2003, 2005; Zhang et al., 2004), resulting in different relative angles between the main axes of the two domains, and this flexibility is believed to be important for the biological function of the molecule.

The DI/DIII Linker

DI and DIII are connected via a flexible linker, spanning the region between the strictly conserved residues Pro283 and Pro294. The conformation of this segment changes radically in the transition to the fusogenic E1 homotrimer (Gibbons et al., 2004), whereas the rest of the molecule roughly maintains its tertiary structure. In the monomer, the only secondary structure adopted by the linker is the short η3 helix. DIII packs against DI via the C and C′ strands, which interact with strands C_0, D_0, and E_0, all in one face of the DI β sandwich. The residues participating in this contact, including a salt bridge, are all polar. This interaction is described in more detail below, in the context of the description of the lateral E1 contacts at the particle surface.

Distribution of Histidines on the E1 Molecule

The pH threshold for the conformational transition of E1 into its fusogenic form corresponds roughly to the pK of histidine (i.e., about pH 6.8). It is thus possible that protonation of a few histidine residues, both in E1 and E2, could play a role in triggering dissociation of the E1/E2 heterodimer. Protonation of some key histidines might also destabilize lateral E1/E1 contacts in the icosahedral particle, helping E1 to rearrange and cause fusion. Figure 1A shows the distribution of histidines in the E1 monomer, highlighting the conserved ones. Mutagenesis experiments have shown that mutation of the conserved His230 (in the ij loop) leads to a fusion block at a late stage, and that the conformational change leading to homotrimer formation is not affected (Chanel-Vos and Kielian, 2004). These experiments point to an important role of the ij hairpin during fusion, and they also suggest that the trigger-sensitive histidines must be located elsewhere. The other strictly conserved histidines are His125, His3, and His386 (the latter His386 is disordered in the structure, but it would be located near the C-terminal residue 384 in the atomic model). In addition, His331 is conserved in E1 from all alphaviruses, except for the eastern equine encephalitis virus (EEEV). However, the reported E1 sequence of this virus has the conserved Cys328, involved in disulfide bond 8 with Cys370, also

(C) Amino acid sequence alignment of E1 proteins from representative alphaviruses: Ross river virus (RRV), O'nyong-nyong virus (NYO), Venezuelan equine encephalitis virus (VEE), western equine encephalitis virus (WEE), Sindbis virus (SIN), and rainbow trout sleeping disease virus (SDV). The secondary structure is represented above the sequence, colored coded as in (A) and (B). Highly and relatively conserved residues are drawn in white font on red background and vice versa, respectively, with variable positions in black. The glycosylation site is marked by a yellow fan as in (A). Cysteines are labeled in green with the number of the disulfide bridge that they form (1–8, as in [A]). Insertions in the amino acid sequence of E1 from the fish alphaviruses (SDV) are numbered in gray to match the arrows in (A). Other symbols underneath the alignment show E1/E1 (triangles) and E1/E2 (blue stars) contacts on the virus particle, determined as indicated in the Experimental Procedures. Yellow triangles denote E1/E1 contacts about the I5 and Q6 axes (Figure 2), and white triangles denote contacts about the Q2 axes. A vertical open arrow above the sequence marks the last amino acid with visible electron density in the crystal (K384). The C-terminal TM region is boxed.

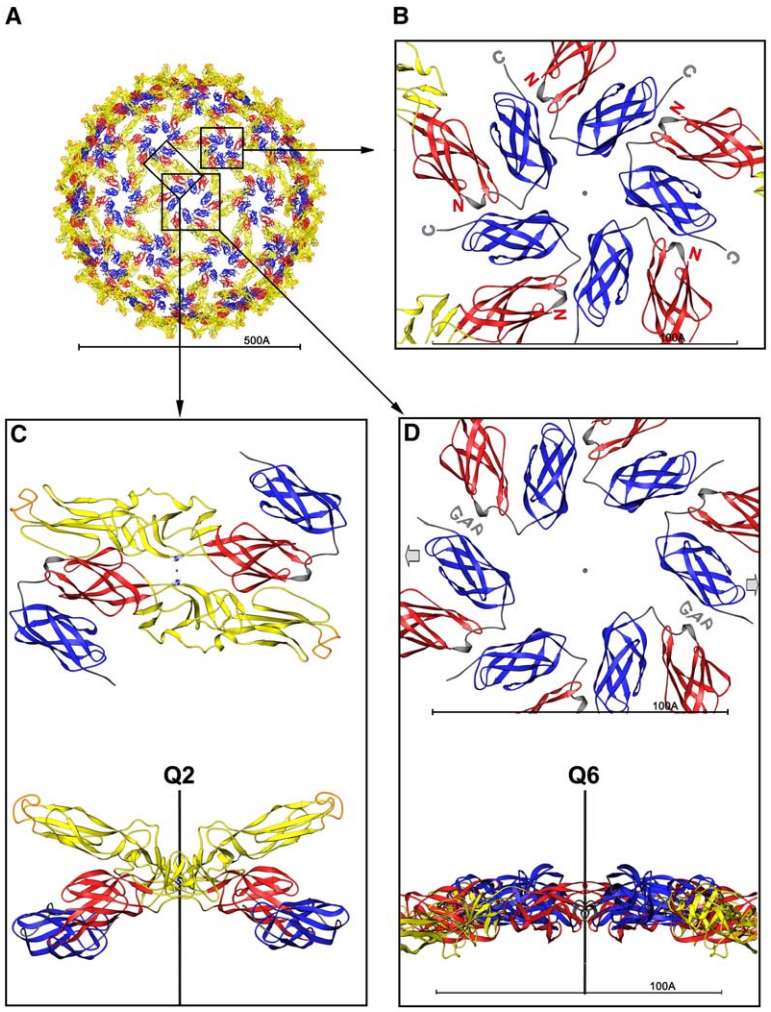

Figure 2. E1 Contacts on the Virus Particle

(A) Overall diagram of the E1 protein shell at the surface of SFV. This diagram serves as reference for the description of the contacts provided in the text; it is equivalent to the one presented by Lescar et al. (2001), except that the Cα trace was replaced by the current E1 model. Squared and rectangular boxes indicate zoom sections displayed.

(B) I5 contacts, with the N and C termini labeled for all five subunits. Each contact involves the AB β hairpin of DIII from one subunit contacting the DI N- and C-terminal ends and the DI/DIII linker of the clockwise subunit. The area buried in the contact is 565 Å^2 per subunit.

(C) Q2 contacts, relating spikes laterally at the virus surface. Top and bottom panels show two orthogonal views, along and perpendicular (respectively) to the Q2 axis. This contact, zoomed in Figure 3B, buries a total of 506 Å^2 per subunit, in two symmetric patches at either side of the Q2 axis.

(D) Q6 contacts. Top and bottom panels are views along and perpendicular to the Q6 axis, respectively. The Q6 axis is coincident with an icosahedral 2-fold axis (I2), which relates two sets of three E1 subunits, with a gap between them (labeled). The contacts within each set are made by the same residues as those of the I5 contact, albeit with a slightly smaller buried surface (498 Å^2 per subunit). Two gray arrows at each side point to a hole in the skirt of the particle (clearly seen in the cryo-EM reconstruction, Mancini et al., 2000). These panels correspond to views from inside the particle drawn in (A).

mutated to valine. Cys370 is still present, resulting in an odd number of cysteines in the ectodomain. Because the disulfide bonds are otherwise strictly conserved in the ectodomains of all alphaviruses (and of all flaviviruses), it is possible that there might have been a sequencing error around residue 330. In SFV, the conserved His331 is part of a cluster, formed also by His333 and His18. Although this cluster is not conserved, all alphaviruses display at least one histidine residue at this interface. Even in EEEV, there is a histidine at position 28, right before strand D0, the imidazole ring of which would be positioned in the area of the 3-His cluster illustrated in Figure 1. The structure thus points to relatively straightforward site-directed mutagenesis experiments to identify the role of each histidine residue or cluster of residues in the pH sensitivity of the alphavirus particle to low pH.

Mapping of Mutations Affecting the Lipid Dependence of Fusion

Alphaviruses have a strict requirement for the presence of specific lipids—cholesterol and sphingolipids—in the target membrane in order for the fusion peptide to insert and drive membrane fusion (reviewed by Kielian et al., 2000). Mutants obtained by passaging SFV in cholesterol-depleted insect cells show a less strict requirement for this lipid. The corresponding mutations are single amino acid changes in E1 that map to three positions. One is Pro226 (Vashishtha et al., 1998) at the tip of the ij loop, right at the interface with the cd loop, in the region of the protein that interacts with the lipid heads during membrane fusion. The other mutants map to positions 44 and 178 (Chatterjee et al., 2002) in the central β sheet of DII. These mutations, depicted in Figure 1A, apparently point to a link in the lipid composition of the target membrane and flexibility at the central β sheet. This connection is perhaps a clue to understanding the complex dynamics of the membrane fusion process, in which membranes of different lipid composition apparently require different levels of flexibility at the hinge. These observations can be related also to the data available on flaviviruses, in which many of the mutations that affect the pH of the fusogenic transition also map to the hinge area (Modis et al., 2003, 2005; Rey et al., 1995).

Organization of the SFV External Glycoprotein Shell

A total of 240 E1/E2 heterodimers associate to form 80 trimers that interact laterally to make a continuous icosahedral shell at the virus surface, almost completely covering the viral membrane. The refined model was initially superposed to the Cα trace (the overall rms deviation of the superposition was 1.3 Å, see legend to Figure S3),

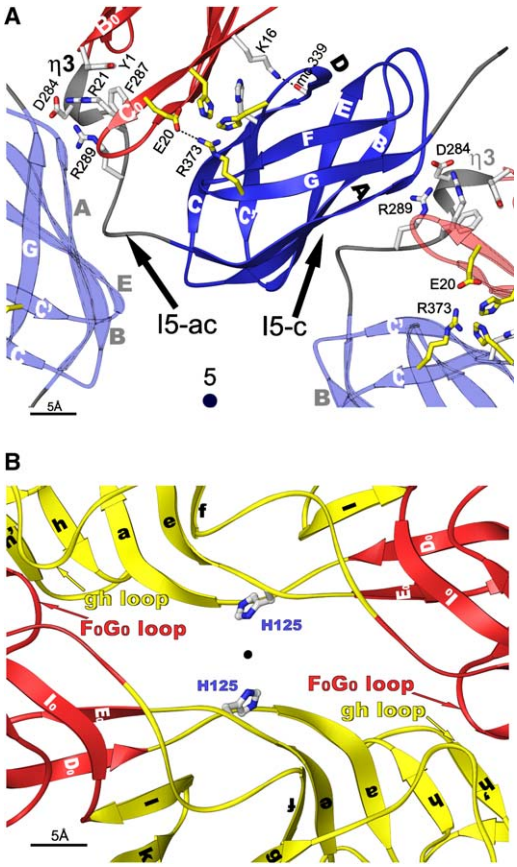

Figure 3. Conserved Residues at the E1/E1 Contacts in the Virus Particle

(A) Details of the interactions about the I5 axes. The subunits are shown in semitransparent colored ribbons, except for one to highlight its contacts with its clockwise and anticlockwise neighbors (the contacts are labeled I5-c and I5-ac, respectively). Selected side chains (according to conservation criteria, see alignment in Figure 1C) are drawn as ball-and-stick and are colored according to atom type: red and blue for oxygen and nitrogen atoms, and white and yellow for carbon atoms from conserved and less conserved amino acids, respectively. Side chains in the intrasubunit contact between DI and DIII are also displayed (note the cluster of histidines already depicted in Figure 1A). "mc339" denotes the main chain carbonyl of residue 339. In the intersubunit contact, Arg289 and Asp284 apparently contact the main chain of strand A of DIII in the neighboring subunit; no conserved side chain of DIII participates in the contact.

(B) E1 interactions at the Q2 axis. The imidazole rings of the conserved His125 are at a distance of about 5–6 Å from each other. The two symmetric contact areas involve DI residues in the F_0G_0 loop (marked by a red arrowhead), interacting with a segment of the gh loop of DII from the opposite subunit (yellow arrowhead). The total buried surface in the contact is 506 $Å^2$ per subunit.

and then its positioning was refined with respect to the cryo-EM electron density after dividing the four E1 subunits of the icosahedral asymmetric unit into nine rigid bodies as described in Lescar et al. (2001). This refinement, using exactly the same procedure used previously to fit the preliminary Cα trace, resulted in essentially the same statistics (R = 33.6 and a correlation coefficient of 89.88%) and an overall rms displacement of the nine rigid bodies of 0.62 Å from the locations obtained by superposing to the previous model (this result is not surprising, given that the overall shape of the initial trace was not altered in the refined model, as shown in Figure S3). The resulting pseudo atomic model of the SFV E1 shell was used to investigate the intersubunit contacts in the virus particle. Although the resolution of the cryo-EM map does not allow for a direct observation of the interactions, several reasonable interpretations can be made based on the residues present at the intersubunit contacts in the pseudo atomic model. All of the E1 amino acids observed in the E1/E1 and E1/E2 contacts are indicated underneath the sequence alignment of Figure 1C.

E1/E1 Contacts

The alphavirus T = 4 surface icosahedral lattice is formed by 80 $(E1/E2)_3$ heterohexameric spikes that interact with each other exclusively via E1/E1 contacts. There are three different types of contacts: about the icosahedral 5-fold (I5) axes, the quasi 6-fold (Q6) axes, and the quasi 2-fold (Q2) axes of the particle (Figure 2). As expected for a shell that has to disassemble easily upon low pH exposure, each of the observed contacts involves polar side chains and buries a modest surface from solvent accessibility, ~500–600 $Å^2$ per contacting subunit. As seen in Figure 2, the I5 and Q6 contacts are very similar (compare [B] and [D]), with a slightly different orientation of DIII with respect to DI in the subunits at the I5 axes. At the Q6 axes, there are two sets of three interacting subunits, with I5-like contacts within each set, and a gap separating the two sets, as indicated in Figure 2D. The presence of this gap is likely to have a functional role, by leaving a space that could allow DIII to glide out as a first disassembly step accompanying E1/E2 dissociation upon exposure to low pH. This putative initial displacement of DIII is indicated by the gray arrow in Figure 2D.

A subset of the side chains present at the I5 and Q2 contacts, which appear important because of their relative conservation among alphaviruses (see Figure 1C), are displayed in Figure 3. This figure also displays side chains in the intrasubunit contact between DI and DIII, since, at the I5, there are alternating intra- and intersubunit contacts involving DI, DIII, and the linker between them. Conserved residues are drawn in white, and less conserved ones are yellow. In the intrasubunit contact, there is the cluster of histidines displayed in Figure 1, a salt bridge between Arg373 (DIII) and Glu20 (DI), and an interaction between the tip of DI Lys16 with the main chain of DIII. Indeed, the side chain of Lys16 exhibits clear electron density and is in position to donate a hydrogen bond to the main chain carbonyl of residue 339 in strand D of DIII. It is interesting to note that in all alphaviruses in which the salt bridge residues Arg373 and Glu20 are not conserved, there is the almost systematic presence of Lys327 in DIII and Glu139 in DI (SFV numbering), which can make a salt bridge equally well when modeled on the SFV E1 structure (in the SFV sequence, these residues are Asp327 and Asn139).

At the I5 intersubunit contact, we note an interesting patch of conserved residues grouped together around the η3 turn in the DI/DIII linker (in gray in the figure). In this cluster, Arg289 and Asp284 apparently contact the main chain of strand A of DIII in the neighbor (counterclockwise) E1 subunit. In addition, a number of intra-DI interactions appear to buttress the side chain of Asp284, which is in position to accept a hydrogen bond from

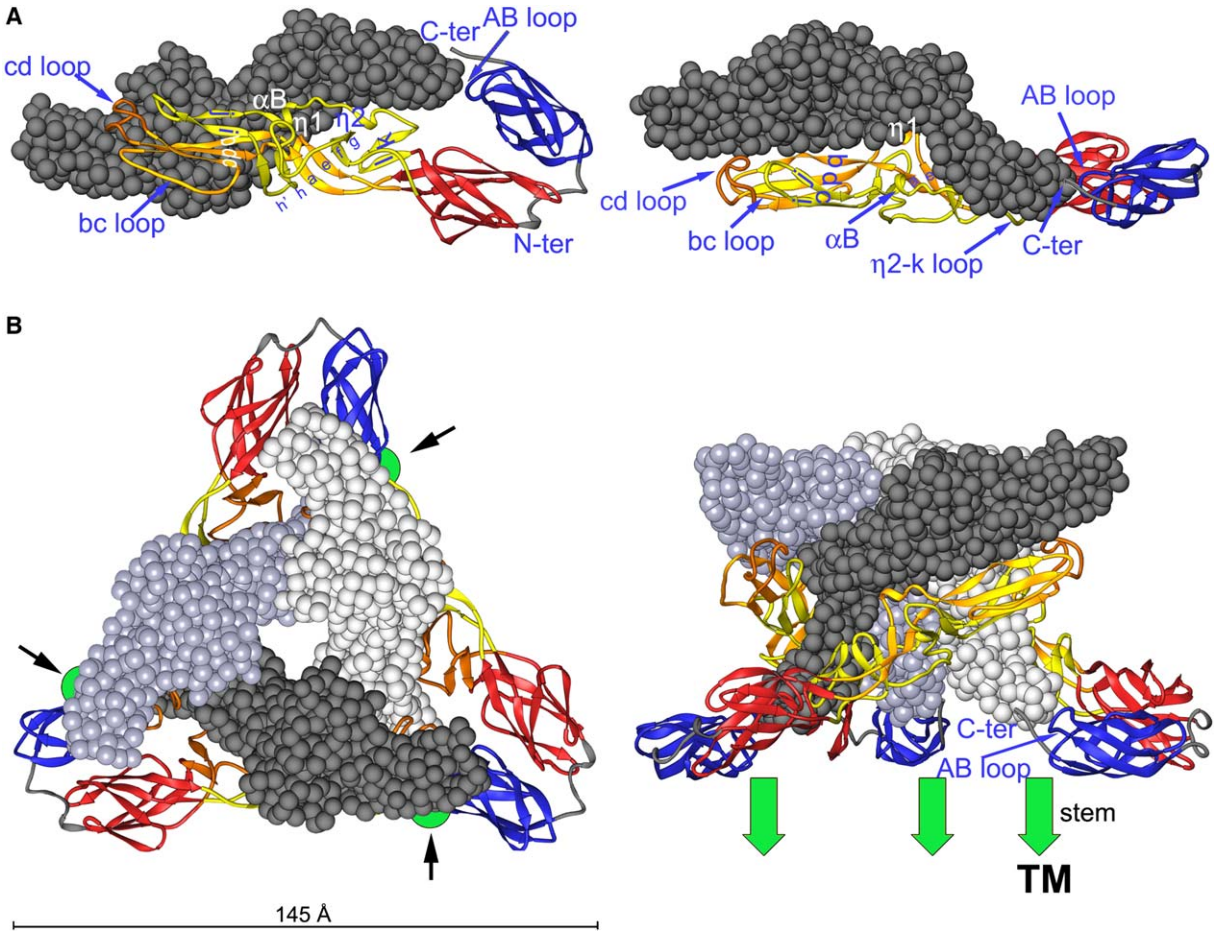

Figure 4. E1/E2 Contacts in the Spike

(A) The ectodomain of the E1/E2 heterodimer is represented with E2 as gray spheres. The crystal structure of E2 is not known, but its volume was recreated by filling the cryo-EM density (Mancini et al., 2000) corresponding to E2 with equally spaced spheres to allow the visualization of the E1 residues that come into contact. Important secondary structure elements of E1 participating in the contact are labeled. The left and right panels are two orthogonal views (looking roughly from the viral membrane and from a side, respectively). Note that DI makes no contacts with E2.

(B) Organization of the $(E1/E2)_3$ complex forming each of the 80 characteristic "spikes" of the virus surface. Left and right panels show two orthogonal views, top (down the 3-fold axis of the spike as seen from outside the particle) and side (the two views are unrelated to those of [A]). Note that all 3-fold interactions are made exclusively by E2. The location of the three "stem regions" (which are absent from the structure but present in the cryo-EM 3D reconstruction), which connect each heterodimeric subunit of the spike to the E1/E2 TM segments, is indicated by three green arrows in the right panel (one of them is labeled). In the left panel, small, black arrows point roughly to the location of the cylindrical green arrows of the right panel.

the strictly conserved Arg21 side chain, which, in turn, makes a stacking interaction with the phenol ring of the N-terminal tyrosine (Tyr1). The latter two side chains are directly in contact with the nonpolar core of dI, via their interaction with Phe287. This set of interactions is completely rearranged after the fusogenic conformational change of E1, disrupted by the extension of the DI/DIII linker to allow for formation of the trimeric E1 hairpin (Gibbons et al., 2004). In the trimer, residues Phe287 and Arg289 move to the new J_0 strand formed by the linker, running antiparallel to strand C_0. Tyr1 does not interact with Arg21 any more, projecting away from the DI hydrophobic core.

The Q2 contacts relating the E1/E2 trimeric spikes laterally also involve residues from E1 only. The amino acids observed at the interaction site are from loop F_0G_0 in DI (residues 149–152) and pack against a portion of the long gh loop (191–196) of DII in the opposite subunit. There is an interesting cluster of aromatic and histidine residues at this contact, depicted in Figure 3B. On the Q2 axis, the side chains of residues Thr41 and Asn43, from the loop between strand D_0 in DI and strand a in DII (i.e., right at the DI/DII interface, in the hinge region), come into contact with each other. Interestingly, the Q2 axis brings the conserved His125 residues from the opposing subunits face to face, with the imidazole rings lying at a distance of about 5–6 Å, within the range of electrostatic repulsion once protonated upon exposure to an acidic environment.

E1/E2 Contacts in the Particle

Fitting E1 into the cryo-EM reconstruction also reveals the location and shape of E2. In contrast to most alphaviruses, many strains of SFV carry the E3 polypeptide. However, the particular strain used for the cryo-EM reconstruction apparently does not contain E3 (E. Mancini and S.D. Fuller, personal communication). All of the

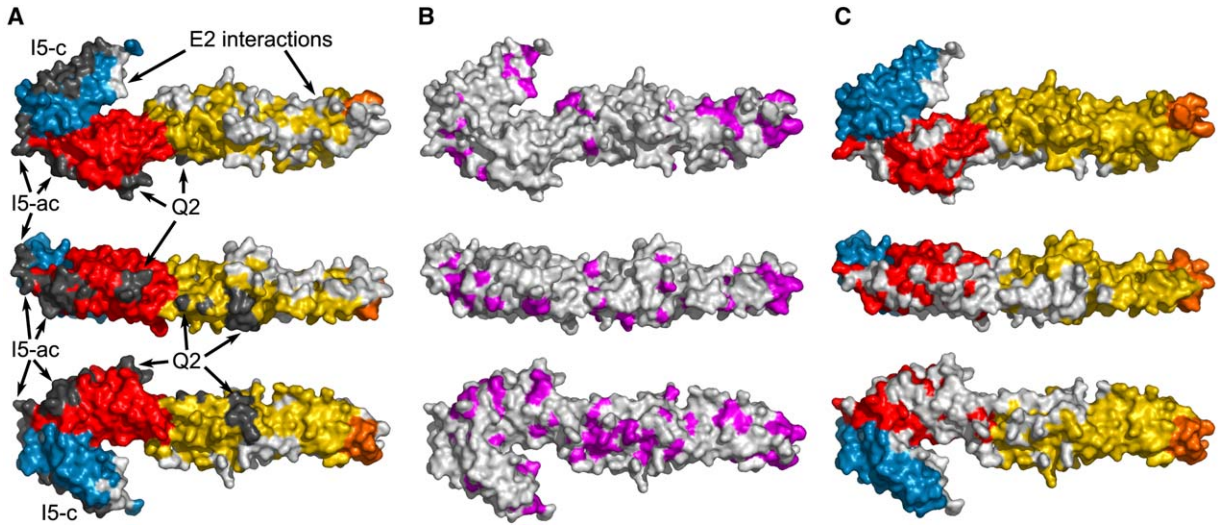

Figure 5. Interaction Surfaces of E1 in the Viral Particle

The E1-ΔS atomic model is drawn in surface representation. Top, middle, and bottom rows show orthogonal views from above, side, and below (i.e., from the viral membrane), respectively, of E1 as it lies on the virion.

(A) Imprint of E2 and the neighboring E1 subunit. The E1-ΔS molecular surface is colored according to domains, and imprints from neighboring E2 and E1 subunits in the particle are shown in white and gray, respectively. I5-c and I5-ac indicate clockwise and anticlockwise E1 contacts at the I5 axes, with reference to the orientation shown in Figure 3A, and Q2 indicates the 2-fold contacts displayed in Figure 3B.

(B) Conserved and nonconserved regions of E1 are shown in magenta and white, respectively.

(C) E1 is displayed as in (A), and the surface amino acids that become buried in the fusogenic E1 homotrimer are painted white. Note that DII has alternative surfaces for contacts with E2 in the particle and with E1 subunits in the postfusion trimer. The latter surface is also the most conserved one (compare with [B]).

extra density can therefore be attributed to E2 and to the stem region of E1 (amino acids 382–413). The EM map clearly shows that the C-terminal TM segments form single density rods across the lipid bilayer, suggesting that the E1/TM and E2/TM α helices interact parallel to each other. The TM helices have indeed been modeled to fit the cryo-EM density in the case of Sindbis virus (Zhang et al., 2002).

Figure 4 shows a model for E2 obtained by filling the extra density in the spike with spheres, corresponding to the E2 ectodomain (excluding the stem region in which the E1 and E2 polypeptides appear to be intimately associated; the two proteins cannot be resolved at the resolution of the cryo-EM map). Figure 4A shows that the C-terminal end of the ectodomain of both polypeptides in the heterodimer come together at one end, where they are continued by the stem and TM regions. The major contact is provided by the conserved AB loop of DIII, in addition to the stem region. The more bulky E2 N-terminal domain interacts with E1/DII at the opposite end of the heterodimer, leaving a hole in between. DII makes extensive contacts with E2, involving mainly the long b β strand and the preceding η1 helix (see Figure 1 for nomenclature). The ij loop and part of the j strand are also seen in the contact, as is the η2 helix and the η2-k loop. Finally, the cd loop interacts extensively with E2. The cryo-EM map indicates that the cd loop is more extended in the contact than it is in the monomer, where it would have to unwind in order to better fit in this region of the map. The cd loop thus apparently folds back on itself upon dissociation of the heterodimer, perhaps to mask the nonpolar side chains of the fusion peptide from solvent. This loop is also observed to be unwound in the crystal structure of the E1 homotrimer, which was crystallized in the presence of nonionic detergents after solubilization from liposomes into which it had been inserted by acidic pH treatment.

Figure 4B shows the organization of the trimer of E1/E2 heterodimers, forming each of the 80 spikes of the T = 4 surface lattice. This figure shows that all of the 3-fold contacts are exclusively mediated by E2, leaving the contacts between spikes to E1. The location of the stem segments and TM regions are indicated by green arrows (right panel) with a circular cross-section when seen from above (left panel). The right panel of this figure shows that the C-terminal two amino acids of E1 (383 and 384), which correspond to the beginning of the stem, are likely to switch directions upon interaction with E2 and point down toward the arrow and reach the viral membrane. In the conformation of the E1 monomer, as seen in the crystal structure, these two residues enter EM density that appears to correspond to E2.

Alternative E1 Interacting Surfaces

Figure 5 summarizes all of the observed interaction surfaces of the E1 molecule in the virus particle (left panel), comparing them to the distribution of conserved surfaces in the molecule (middle panel) and with the surfaces involved in contacts within the fusogenic E1 homotrimer (E1HT). It is clear that the most conserved surface of E1 faces the viral membrane in the particle and is buried at the E1*HT interface. In the particle, the less conserved outward facing surface of DII interacts with E2. In contrast to DII, which displays alternative surfaces for E1/E2 contacts in the particle and E1/E1 interactions within the trimer, the DIII surface that is in contact with E2 in the virion is the same as that involved in inter- and intrasubunit interactions in E1*HT, particularly the highly conserved AB loop. Figure 5 also shows that the

Table 3. TLS Matrices from REFMAC

TLS Chain A								
Range	"1"	"289"	All					
Origin	−12.708	51.653	171.765					
T	0.7646	0.1518	0.1139	−0.1969	−0.1680	0.0940		
L	1.9396	1.3447	15.7642	0.7149	−4.0373	−2.6792		
S	−1.0877	0.7956	0.1654	−0.4139	0.0164	0.1736	−0.3230	−1.3362
TLS Chain B								
Range	"290"	"384"	All					
Origin	−38.097	41.054	217.214					
T	0.9151	0.9271	0.9273	0.0182	0.0174	0.0499		
L	3.6040	8.6947	19.6051	4.9019	5.0578	−0.3157		
S	1.1529	−1.2722	0.1537	0.7379	1.9061	0.2863	−1.9592	−2.3632

exposed surfaces of DI and DIII in the particle are essentially also exposed in the E1 homotrimer. This is similar to the case of the flavivirus E trimer, in which the buried surfaces in the trimer are also buried or facing the virus membrane in the virus particle (Bressanelli et al., 2004; Modis et al., 2004).

Conclusion

The data reported in this manuscript provide a description of the flexible E1 subunit of the SFV particle, crystallographically refined to as far as the quality of the diffraction permits. The independent tests and independently observed structure of the E1*HT, as well as the very good fit of the monomer into the medium-resolution (9 Å) cryo-EM map of the whole particle, lend support to the interpretation of the structure. The resulting model shows an apparently nonrandom distribution of histidine residues, which is likely to be relevant for understanding the sensitivity of the E1/E2 assembly to acidification. The E1 structure allows for the mapping of the cholesterol-sensitivity mutations, which, in turn, point to an apparent link between flexibility at the hinge region and lipid composition of the target membrane in order to drive membrane fusion. In addition, this work provides an envelope for the E2 ectodomain, and it shows that E2 is exclusively responsible for all of the 3-fold interactions in the particle. Thus, no 3-fold contacts between E1 subunits are possible in the organization of the virus particle at neutral pH, precluding any premature E1 homotrimerization. A more thorough interpretation of the contacts forming the SFV particles now awaits the determination of the atomic structure of E2. Finally, a number of conserved amino acids of E1 appear to be located at strategic locations at the interaction sites in the particle, around I5 and Q6 axes, and about the Q2 axes relating adjacent spikes. A gap at the Q6 contacts between E1 subunits is postulated to provide an initial disassembly path, concomitant with E1/E2 heterodimer dissociation and before trimerization of E1.

Experimental Procedures

E1 Crystals

The procedures followed for the purification and crystallization of E1 from the virus have been reported earlier (Wengler et al., 1999). The crystal used for refinement has space group $P6_422$ with unit cell dimensions a = 79.8 Å, c = 335.8 Å at 100 K and one E1 molecule per asymmetric unit (Vm = 3.2 $Å^3$/Da and a solvent content of 62%).

Native Data Collection and Structure Determination

Data collection and processing have been described (Lescar et al., 2001). Briefly, all images were processed with DENZO and SCALEPACK (Otwinowski and Minor, 1997). No anisotropic correction was made to the diffraction data, but an anisotropic overall B factor was used in refinement. The initial model was subjected to alternate cycles of molecular dynamic refinement with program CNS (Brünger et al., 1998), by using the parameter set of Engh and Huber (1991), and manual model building with the programs QUANTA (Molecular Simulations, Inc.) and O (Jones and Kjeldgaard, 1997). The R_{free} (Brünger and Rice, 1997) was used to monitor the progress of the refinement by omitting 10% of the data (1286 reflections), randomly selected, throughout the procedure. Refinement was further pursued by using REFMAC with the TLS option (Winn et al., 2003) to model pseudo rigid body displacements within the crystal, which was crucial to bring the R_{free} to below 32%. Two TLS groups were defined (domains I+II and domain III) (Table 3). Figure S4 shows a plot of the B factor and the TLS contribution for each amino acid. For calculating the "radiation-induced" difference electron density map (Figure S2), two native data sets were collected consecutively by using the same crystal with an attenuated beam. Between the first (Fnonirr) and second (Firr) data set, the crystal was exposed for 30 s to the unattenuated beam. Difference electron density maps were subsequently calculated by using Fourier amplitudes Fnonirr-Firr and phases from the refined model.

Determination of the E1/E1 and E1/E2 contacts was made with CONTACT of the CCP4 suite, by using a sphere with a radius of 4 Å within which neighboring atoms from different subunits where counted as in contact. For the E1/E2 contacts, the coordinates of the spheres displayed in Figure 4 were used, and, in this case, a radius of 5 Å was used.

Supplemental Data

Supplemental Data including an experimental confirmation of the location of disulfides and carboxylates in the model by means of a difference electron density map between fresh and an irradiated crystal, as well as an analysis of the thermal factors of the new model and a comparison with the previously published Cα trace, are available at http://www.structure.org/cgi/content/full/14/1/75/DC1/.

Acknowledgments

This work was supported by the Centre National de la Recherche Scientifique (CNRS), with additional help from program SESAME of the "Région Ile-de-France" and from a Human Frontiers Science Program grant (to F.A.R.). All diffraction data collection experiments were carried out at the European Synchrotron Radiation Facility (ESRF), Grenoble, France. We thank the ESRF/European Molecular Biology Laboratory "Joint Structural Biology Group" in Grenoble for help and discussion, and M. Kielian for comments on the manuscript.

Received: June 21, 2005
Revised: September 19, 2005
Accepted: September 19, 2005
Published: January 10, 2006

References

Andersson, H., Barth, B.U., Ekstrom, M., and Garoff, H. (1997). Oligomerization-dependent folding of the membrane fusion protein of SFV. J. Virol. *71*, 9654–9663.

Bressanelli, S., Stiasny, K., Allison, S.L., Stura, E.A., Duquerroy, S., Lescar, J., Heinz, F.X., and Rey, F.A. (2004). Structure of a flavivirus envelope glycoprotein in its low-pH-induced membrane fusion conformation. EMBO J. *23*, 728–738.

Bron, R., Wahlberg, J.M., Garoff, H., and Wilschut, J. (1993). Membrane fusion of SFV in a model system: correlation between fusion kinetics and structural changes in the envelope glycoprotein. EMBO J. *12*, 693–701.

Brünger, A., and Rice, L. (1997). Crystallographic refinement by simulated annealing: methods and applications. Methods Enzymol. *277*, 243–269.

Brünger, A., Adams, P., Clore, G., DeLano, W., Gros, P., Grosse-Kunstleve, R., Jiang, J., Kuszewski, J., Nilges, M., and Pannu, N. (1998). Crystallography and NMR system: a new sofware suite for macromolecular structure determination. Acta Crystallogr. D Biol. Crystallogr. *54*, 905–921.

Caspar, D.L., and Klug, A. (1962). Physical principles in the construction of regular viruses. Cold Spring Harb. Symp. Quant. Biol. *27*, 1–24.

Chanel-Vos, C., and Kielian, M. (2004). A conserved histidine in the ij loop of the SFV E1 protein plays an important role in membrane fusion. J. Virol. *78*, 13543–13552.

Chatterjee, P.K., Eng, C.H., and Kielian, M. (2002). Novel mutations that control the sphingolipid and cholesterol dependence of the SFV fusion protein. J. Virol. *76*, 12712–12722.

de Curtis, I., and Simons, K. (1988). Dissection of SFV glycoprotein delivery from the trans-Golgi network to the cell surface in permeabilized BHK cells. Proc. Natl. Acad. Sci. USA *85*, 8052–8056.

Engh, R.A., and Huber, R. (1991). Accurate bond and angle parameters for X-ray protein structure refinement. Acta Crystallogr. A *47*, 392–400.

Flores, T.P., Moss, D.S., and Thornton, J.M. (1994). An algorithm for automatically generating protein topology cartoons. Protein Eng. *7*, 31–37.

Gaedigk-Nitschko, K., and Schlesinger, M.J. (1990). The Sindbis virus 6K protein can be detected in virions and is acylated with fatty acids. Virology *175*, 274–281.

Garoff, H., Wilschut, J., Liljestrom, P., Wahlberg, J.M., Bron, R., Suomalainen, M., Smyth, J., Salminen, A., Barth, B.U., Zhao, H., et al. (1994). Assembly and entry mechanisms of SFV. Arch. Virol. Suppl. *9*, 329–338.

Gibbons, D.L., Erk, I., Reilly, B., Navaza, J., Kielian, M., Rey, F.A., and Lepault, J. (2003). Visualization of the target-membrane-inserted fusion protein of SFV by combined electron microscopy and crystallography. Cell *114*, 573–583.

Gibbons, D.L., Vaney, M.C., Roussel, A., Vigouroux, A., Reilly, B., Lepault, J., Kielian, M., and Rey, F.A. (2004). Conformational change and protein-protein interactions of the fusion protein of SFV. Nature *427*, 320–325.

Hamburger, Z.A., Brown, M.S., Isberg, R.R., and Bjorkman, P.J. (1999). Crystal structure of invasin: a bacterial integrin-binding protein. Science *286*, 291–295.

Harpaz, Y., and Chothia, C. (1994). Many of the Ig superfamily domains in cell adhesion molecules and surface receptors belong to a new structural set which is close to that containing variable domains. J. Mol. Biol. *238*, 528–539.

Helenius, A., Kartenbeck, J., Simons, K., and Fries, E. (1980). On the entry of SFV into BHK-21 cells. J. Cell Biol. *84*, 404–420.

Holm, L., and Sander, C. (1996). Mapping the protein universe. Science *273*, 595–603.

Jones, T.A., and Kjeldgaard, M. (1997). Electron-density map interpretation. Methods Enzymol. *277*, 173–208.

Kielian, M., Chatterjee, P.K., Gibbons, D.L., and Lu, Y.E. (2000). Specific roles for lipids in virus fusion and exit. Examples from the alphaviruses. Subcell. Biochem. *34*, 409–455.

Lee, S., Owen, K.E., Choi, H.K., Lee, H., Lu, G., Wengler, G., Brown, D.T., Rossmann, M.G., and Kuhn, R.J. (1996). Identification of a protein binding site on the surface of the alphavirus nucleocapsid and its implication in virus assembly. Structure *4*, 531–541.

Lescar, J., Roussel, A., Wien, M.W., Navaza, J., Fuller, S.D., Wengler, G., Wengler, G., and Rey, F.A. (2001). The fusion glycoprotein shell of SFV: an icosahedral assembly primed for fusogenic activation at endosomal pH. Cell *105*, 137–148.

Liljestrom, P., Lusa, S., Huylebroeck, D., and Garoff, H. (1991). In vitro mutagenesis of a full-length cDNA clone of SFV: the small 6,000-molecular-weight membrane protein modulates virus release. J. Virol. *65*, 4107–4113.

Luo, Y., Frey, E.A., Pfuetzner, R.A., Creagh, A.L., Knoechel, D.G., Haynes, C.A., Finlay, B.B., and Strynadka, N.C. (2000). Crystal structure of enteropathogenic *E. coli* intimin-receptor complex. Nature *405*, 1073–1077.

Lusa, S., Garoff, H., and Liljestrom, P. (1991). Fate of the 6K membrane protein of SFV during virus assembly. Virology *185*, 843–846.

Mancini, E.J., Clarke, M., Gowen, B.E., Rutten, T., and Fuller, S.D. (2000). cEM reveals the functional organization of an enveloped virus, Semliki Forest virus. Mol. Cell. *5*, 255–266.

Modis, Y., Ogata, S., Clements, D., and Harrison, S.C. (2003). A ligand-binding pocket in the dengue virus envelope glycoprotein. Proc. Natl. Acad. Sci USA *100*, 6986–6991.

Modis, Y., Ogata, S., Clements, D., and Harrison, S.C. (2004). Structure of the dengue virus envelope protein after membrane fusion. Nature *427*, 313–319.

Modis, Y., Ogata, S., Clements, D., and Harrison, S.C. (2005). Variable surface epitopes in the crystal structure of dengue virus type 3 envelope glycoprotein. J. Virol. *79*, 1223–1231.

Mukhopadhyay, S., Zhang, W., Gabler, S., Chipman, P.R., Strauss, E.G., Strauss, J.H., Baker, T.S., Kuhn, R.J., and Rossman, M.G. (2006). Mapping the structure and function of the E1 and E2 glycoproteins in alphaviruses. Structure *14*, this issue, 63–73.

Otwinowski, Z., and Minor, W. (1997). Processing of X-ray diffraction data collected in oscillation mode. Methods Enzymol. *276*, 307–326.

Paredes, A., Alwell-Warda, K., Weaver, S.C., Chiu, W., and Watowhich, S.J. (2001). VEEV structure and its divergence from old world alphaviruses. J. Virol. *75*, 9532–9537.

Pletnev, S.V., Zhang, W., Mukhopadhyay, S., Fisher, B.R., Hernandez, R., Brown, D.T., Baker, T.S., Rossmann, M.G., and Kuhn, R.J. (2001). Locations of carbohydrate sites on alphavirus glycoproteins show that E1 forms an icosahedral scaffold. Cell *105*, 127–136.

Rey, F.A., Heinz, F.X., Mandl, C., Kunz, C., and Harrison, S.C. (1995). The envelope glycoprotein from tick-borne encephalitis virus at 2 Å resolution. Nature *375*, 291–298.

Salminen, A., Wahlberg, J.M., Lobigs, M., Liljestrom, P., and Garoff, H. (1992). Membrane fusion process of SFV II: cleavage-dependent reorganization of the spike protein complex controls virus entry. J. Cell Biol. *116*, 349–357.

Schlesinger, S., and Schlesinger, M. (2001). Togaviridae: the viruses and their replication. In Fields Virology, D.M. Knipe, and P.M. Howley, eds. (Philadelphia: Lippincott Williams and Wilkins), pp. 895–916.

Skoging, U., Vihinen, M., Nilsson, L., and Liljestrom, P. (1996). Aromatic interactions define de binding of the alphavirus spike to its nucleocapsid. Structure *4*, 519–529.

Vashishtha, M., Phalen, T., Marquardt, M.T., Ryu, J.S., Ng, A.C., and Kielian, M. (1998). A single point mutation controls the cholesterol dependence of Semliki Forest virus entry and exit. J. Cell Biol. *140*, 91–99.

von Bonsdorf, C.H., and Harrison, S.C. (1975). Sindbis virus glycoproteins form a regular icosahedral surface lattice. J. Virol. *16*, 141–145.

von Bonsdorf, C.H., and Harrison, S.C. (1978). Hexagonal glycoprotein arrays from Sindbis virus membranes. J. Virol. *28*, 578–583.

Watson, D.G., Moehring, J.M., and Moehring, T.J. (1991). A mutant CHO-K1 strain with resistance to *Pseudomonas* exotoxin A and alphaviruses fails to cleave Sindbis virus glycoprotein PE2. J. Virol. *65*, 2332–2339.

Weaver, S.C., Dalgarno, L., Frey, T.K., Huang, H.V., Kinney, R.M., Rice, C.M., Roehrig, J.J., Shope, R.E., and Strauss, E.G. (2000). Family Togaviridae. In Virus Taxonomy: Seventh Report of the International Committee on Taxonomy of Viruses, M.V. van Regenmortel, C.M. Fauguet, D.H.I. Bishop, E.B. Carstens, M.K. Estes, S.M. Lemon, J. Maniloff, M.A. Mayo, D.J. McGeoch, and C.R. Pringle, et al., eds. (San Diego, CA: Academic Press), pp. 879–889.

Wengler, G., Wengler, G., and Rey, F.A. (1999). The isolation of the ectodomain of the alphavirus E1 protein as a soluble hemagglutinin and its crystallization. Virology *257*, 472–482.

Winn, M.D., Murshudov, G.N., and Papiz, M.Z. (2003). Macromolecular TLS refinement in REFMAC at moderate resolutions. Methods Enzymol. *374*, 300–321.

Zhang, W., Mukhopadhyay, S., Pletnev, S.V., Baker, T.S., Kuhn, R.J., and Rossmann, M.G. (2002). Placement of the structural proteins in Sindbis virus. J. Virol. *76*, 11645–11658.

Zhang, X., Fugere, M., Day, R., and Kielian, M. (2003). Furin processing and proteolytic activation of Semliki Forest virus. J. Virol. *77*, 2981–2989.

Zhang, Y., Zhang, W., Ogata, S., Clements, D., Strauss, J.H., Baker, T.S., Kuhn, R.J., and Rossmann, M.G. (2004). Conformational changes of the flavivirus E glycoprotein. Structure (Camb) *12*, 1607–1618.

Accession Numbers

The E1 coordinates have been deposited in the Protein Data Bank with accession code 2ALA.